2020 IEEE Conference on Control Technology and Applications (CCTA)
August 24-26, 2020. Montréal, Canada

Impacts of Distributed Speed Harmonization and Optimal Maneuver Planning on Multi-Lane Roads*

Nathan Goulet[1] and Beshah Ayalew[1]

Abstract— **A commonly proposed method for improving traffic flow on freeways is speed harmonization. The effectiveness of current speed harmonization approaches, such as variable speed limits, is extremely reliant on human driver compliance. Connected and automated vehicles (CAVs) are expected to come to market within this decade, offering the opportunity to eliminate or reduce the reliance on human compliance. However, extending current roadside infrastructure-based approaches of assigning centrally computed harmonization speeds to individual vehicles is, costly. An alternative approach is to have individual vehicles estimate the traffic state on-board and make distributed decisions to achieve the harmonization goal autonomously. In this work, we present a distributed algorithm for estimating the current average speed of traffic. We couple this with a distributed 2D maneuver planning approach. Then, we study the impact on traffic efficiency in terms of energy consumption and travel time at varying CAV penetration rates.**

I. INTRODUCTION

Within densely populated areas in the United States, the average commuter spends 71 hours of extra travel time per year due to delays [1]. Almost 54% of congestion in these dense areas occurs on freeways [1], presenting a need to significantly decrease the amount of delay by utilizing the existing freeway networks more efficiently. As connected and automated vehicles (CAVs) become closer to reality, there is an opportunity to directly influence individual vehicle control to a level which is not possible with human drivers (HD). However, as we will show later, if the control strategies are not appropriately designed, average travel time can increase. In this paper, we present a distributed control framework for speed harmonization and 2D maneuver planning on multi-lane freeways that exploits CAV technologies to improve traffic efficiency.

A 2D maneuver (or simply maneuver) will be defined as a combined longitudinal and lateral motion plan that encompasses lane and speed selections by individual vehicles. From an individual vehicle's egoistic perspective, optimization techniques are a popular method for solving the maneuver planning problem. These generally fall into three categories: graph search methods [2], [3], sampling-based methods [4], [5], and model predictive control (MPC) [6]–[9]. Graph search methods, such as A* [2], [3], do not necessarily result in optimal plans due to the path discretization. Additionally, graph search methods typically do not consider lane decisions. Sampling-based methods, such as the rapidly-exploring random tree (RRT), have been expanded in [4], [5] to consider lane decisions using particle sampling techniques. RRT based methods do require a complimentary collision checking algorithm, whereas MPC techniques are able to explicitly and intrinsically handle collision avoidance constraints.

Our early work posed an individual vehicle's maneuver planning problem as a hierarchical hybrid control scheme [10] that used a rule-based finite state machine to force a lane change when a set velocity threshold was met. In [6], the problem was reformulated so that the lane decisions were included in the MPC optimizations leading to a mixed-integer problem (MIP) that utilized binary lane decision variables to weight the lane reference speed and centerline tracking costs. The framework was still hierarchical with a reference speed assigner that utilized a set of rules to assign the reference speed in each lane. The computational complexity of this formulation, however, was found to have high-order polynomial growth with respect to the number of lanes and time steps of the prediction horizon. Therefore, the lane decision variables were relaxed to be real-valued, reducing the computational growth to low-order polynomial [11]. Additional MIP formulations in the literature include [7] and [8], which both attempt to change lanes in order to minimize a desired velocity tracking error and accelerations. These differ from our approach as they do not explicitly associate a cost to a given lane. The benefit of assigning a reference speed to track in each lane, is that it offers an opportunity to harmonize traffic speed as we discuss next.

Currently implemented methods for speed harmonization typically utilize infrastructure-based variable speed limit (VSL) and variable messaging systems (VMS) to influence human-driven vehicle (HDV) traffic [12], [13]. Results for VSL mitigating slow-downs and/or increasing safety by reducing the number of incidents have been mixed [13], [14]. The main reason for this is that they rely on HDs and their compliance to the VSL [15]. The introduction of CAVs can alleviate this issue as automated vehicles can be designed to follow computed plans closely. However, as CAVs are likely to be introduced in legacy traffic at different penetrations, they will need to interact with mixed HDV and CAV traffic without negatively impacting the flow. Through the use of coordinated CAVs, the work in [16] was able to reduce speed oscillations in HDV traffic, while [17] showed the potential of speed harmonization through individual vehicle control to reduce travel times by up to 30% via an optimal control strategy with 100% CAVs and restricting lane changes.

**This research was supported by an award from the U.S. Department of Energy Vehicle Technologies Office (Project No. DE-EE0008232)

[1]Nathan Goulet and Beshah Ayalew are with the Applied Dynamics & Control Group at Clemson University - International Center for Automotive Research (CU-ICAR), 4 Research Dr., Greenville, SC 29607 USA {ngoulet, beshah}@clemson.edu

Authorized licensed use limited to: CLEMSON UNIVERSITY. Downloaded on April 17,2022 at 23:29:03 UTC from IEEE Xplore. Restrictions apply.

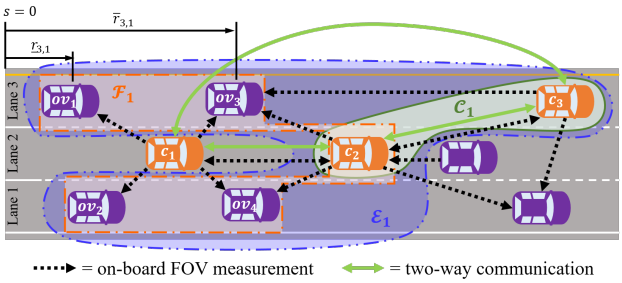

Fig. 1. Example traffic topology highlighting the sets of OVs $\mathcal{C}_1 = \{c_2,\ c_3\}$, $\mathcal{F}_1 = \{ov_1,\ ov_3,\ c_2,\ ov_2,\ ov_4\}$, and $\mathcal{E}_1 = \{ov_1,\ ov_3,\ c_3,\ c_2,\ ov_2,\ ov_4\}$ in the neighborhood of c_1.

In this paper, we present a distributed reference speed assignment algorithm to be coupled with a distributed maneuver planner running on-board the individual CAVs, in order to harmonize traffic flow without needing to invest in roadside infrastructure. Further, we compare the proposed distributed harmonization technique with a rule-based speed assignment to understand how different methodologies of distributed speed assignment may impact traffic. In order to quantify the impacts of the distributed framework, we analyze fuel consumption results, travel time results, and lateral maneuver (lane change) occurrences from large scale traffic microsimulations.

The remainder of the paper is organized as follows: Section II presents the distributed maneuver planning and reference speed assignment framework; Section III presents some results and discussions; and Section IV provides concluding remarks.

II. DISTRIBUTED CONTROL FRAMEWORK

We first define some notations: an object vehicle (OV) may be either a CAV or an HDV, $\mathcal{C}_i$ is the set of all CAVs c_p $(p \neq i)$ communicating with CAV c_i, $\mathcal{F}_i$ is the set of all OVs ov_q within the assumed rectangular field of view (FOV) of c_i, and $\mathcal{E}_i = \mathcal{C}_i \cup \mathcal{F}_i$ is the extended neighborhood of c_i. It should be noted that $\mathcal{C}_i \cap \mathcal{F}_i$ may not be empty. Figure 1 outlines these sets for c_1 within an example traffic scene.

The overall distributed control framework to be implemented on-board a given CAV c_i is outlined with the block diagram in Fig. 2 and select variables are defined in the caption. At the beginning of each update step, ego-vehicle c_i receives an information matrix $\mathbf{w}_p$ from CAV $c_p \in \mathcal{C}_i$ $(p \neq i)$, that includes a trajectory plan, and obtains its own measurements of all $ov_q \in \mathcal{F}_i$. The object vehicle state prediction (OVSP) block utilizes this information in order to predict the future states, $\mathbf{x}_j$, of all $ov_j \in \mathcal{E}_i$. Any appropriate synchronization and/or OVSP method may be utilized for this purpose; in our simulations we utilize the constant velocity synchronization method for all CAVs $c_p \in \mathcal{C}_i$, and the decoupled longitudinal and lateral kinematics OVSP models for all $ov_j \in \mathcal{E}_i \setminus \mathcal{C}_i$ presented in [18]. The next step in the framework is the reference speed assigner (RSA) block, which utilizes shared information and predicted trajectories to assign a reference speed to each lane. We will

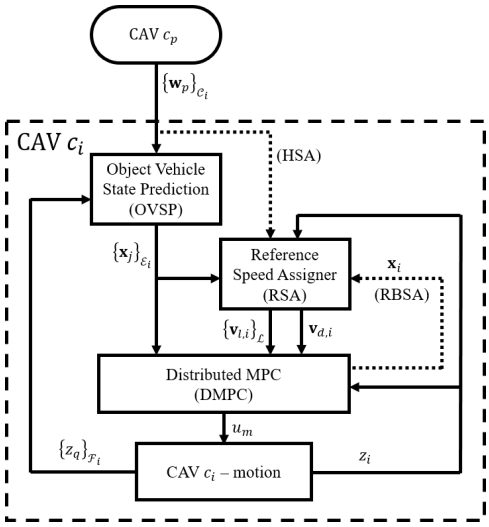

Fig. 2. The control framework for CAV c_i, where the dotted lines labeled RBSA and HSA designate the differences in flow between the two RSA approaches. Further, $\{\mathbf{w}_p\}_{\mathcal{C}_i}$ is the set of all information matrices from CAVs $c_p \in \mathcal{C}_i$, $\mathbf{x}_i$ is the predicted optimal state trajectory for c_i, $\{\mathbf{x}_j\}_{\mathcal{E}_i}$ defines the set of predicted state trajectories for all $ov_j \in \mathcal{E}_i$, $\mathbf{v}_{d,i}$ is the desired velocity of c_i over the prediction horizon, $\{\mathbf{v}_{l,i}\}_{\mathcal{L}}$ is the set of reference velocities estimated by c_i for each lane $l \in \mathcal{L}$ over the prediction horizon, where $\mathcal{L}$ is the set of lanes on the current link, z_i are the measurements about c_i, $\{\mathbf{z}_q\}_{\mathcal{F}_i}$ is the set of measurements about all $ov_q \in \mathcal{F}_i$, and u_m are the inputs associated with the motion dynamics model.

present two methods, rule-based and harmonization-based speed assignment (RBSA and HSA, respectively) in Section II-B. Then the DMPC block receives the state measurements of CAV c_i, the predicted trajectories of each $ov_j \in \mathcal{E}_i$, and the assigned reference speeds from the RSA block in order to plan an optimal trajectory for the ego-vehicle. The details of the DMPC formulation will be presented below. The optimal control inputs are then passed to the lower level vehicle dynamics controller.

A. Distributed Model Predictive Control Formulation

The multi-objective DMPC problem to be solved at each CAV c_i can be written compactly as:

$$\min_{\mathbf{u}_i} \|\mathbf{F}_i\|^2_{\mathbf{P}_{f,i}} + \|\mathbf{G}_i\|^2_{\mathbf{P}_{g,i}} + \|\mathbf{H}_i\|^2_{\mathbf{P}_{h,i}} + \|\mathbf{u}_i\|^2_{\mathbf{R}_i} \tag{1a}$$

$$s.t.\ \ x_{i,k+1} = f\left(x_{i,k}, u_{i,k}\right),\ x_{i,k} \in X_i,\ u_{i,k} \in U_i \tag{1b}$$

$$x_{i,0} = \hat{x}_{i,0} \tag{1c}$$

$$c(x_{i,k}, u_{i,k}) \geq 0 \tag{1d}$$

$$g(x_{i,k}, x_{j,k}) \geq 0\ \forall\ ov_j \in \mathcal{E}_i, \tag{1e}$$

where $x_{i,k}$ is the state vector of c_i at the prediction time step k, and $\mathbf{u}_i = \begin{bmatrix} u_{i,0} & u_{i,1} & \cdots & u_{i,N_h-1} \end{bmatrix}^T$ is the matrix of control vectors $u_{i,k}$ over the prediction horizon with N_h steps. The cost function is the sum of the weighted 2-norms of the lane-dependent $\mathbf{F}_i$, the lane-independent $\mathbf{G}_i$ and the predictability $\mathbf{H}_i$ output vectors, as well as, the input vector $\mathbf{u}_i$, where we define the weighted 2-norm $\|\mathbf{F}\|^2_{\mathbf{P}} = \mathbf{F}^T\mathbf{P}\mathbf{F}$. The output vectors are of the form $\mathbf{F}_i = \begin{bmatrix} F_{i,1}, & \cdots, & F_{i,N_h} \end{bmatrix}^T$, however, the predictability output vector terminates at $N_h - 1$, as there is no

Authorized licensed use limited to: CLEMSON UNIVERSITY. Downloaded on April 17,2022 at 23:29:03 UTC from IEEE Xplore. Restrictions apply.

terminal predictability cost. The respective weighting matrices $\mathbf{P}_{f,i}$, $\mathbf{P}_{g,i}$, $\mathbf{P}_{h,i}$ and $\mathbf{R}_i$ are of the form $\mathbf{P}_i = \text{diag}\left\{P_{i,1}, \quad \cdots, \quad P_{i,N_h}\right\}$ with appropriate length, where the weighting matrix at a given time step $P_{i,k}$ is symmetric, positive semi-definite, and of appropriate dimensions. The optimal control problem is subject to the state dynamics equation $f\left(x_{i,k}, u_{i,k}\right)$, and to the admissible set of states X_i, and inputs U_i, as noted in (1b). We have utilized the dynamic particle motion model presented in [19] and modified in [18] (see Fig. 3 for notations). However, other models, such as the kinematic or dynamic bicycle model, may be used. Let $\hat{x}_{i,0}$ in (1c) be the initial state estimate at the current time. Further, the problem is subject to additional vehicle and road constraints $c\left(x_{i,k}, u_{i,k}\right)$ in (1d), and obstacle avoidance constraints $g\left(x_{i,k}, x_{j,k}\right)$ in (1e), whose discussion will be omitted for brevity. The interested reader may find detailed discussions of all constraints in [18], [19].

In the following, we will discuss the different components of the cost function in further detail. In order to reduce clutter, we will hereafter drop the time index k, and ego-vehicle index i, except where we need to distinguish between the ego and other vehicles.

1) Lane-Dependent Cost: The lane-dependent output vector is given by [11]:

$$F = [d_1\left(y_e - y_{e,1}\right), \quad \cdots, \quad d_{N_l}\left(y_e - y_{e,N_l}\right), \\ d_1\left(v - v_1\right), \quad \cdots, \quad d_{N_l}\left(v - v_{N_l}\right)]^T, \quad (2)$$

where y_e is the deviation from the path centerline of CAV c_i, v is the tangential velocity of CAV c_i, and d_l is a decision variable that weights the tracking errors associated with the given lane l. Further, $y_{e,l}$ and v_l are the lane centerline and lane reference velocity, respectively, while N_l is the total number of lanes on the link. Figure 3 depicts a three lane road to clarify select variables.

We define the lane decision variables to be constrained such that $d_l \in \begin{bmatrix}0, & 1\end{bmatrix}$ and:

$$\sum_{l=1}^{N_l} d_l = 1, \quad (3)$$

in order to ensure a normalized weighting of lane tracking errors. We then manipulate the lane decision variables with the integrator dynamics:

$$d_{l,k+1} = d_{l,k} + u_{l,k}\Delta t \quad \forall\, l \in \{1, ..., N_l - 1\}, \quad (4)$$

where u_l for all $l \in \{1, ..., N_l - 1\}$ are control variables [11] and Δt is the time step. In order to reduce the number of control variables by one, we define the last lane decision varible d_{N_l} algebraically as:

$$d_{N_l} = 1 - \sum_{l=1}^{N_l - 1} d_l. \quad (5)$$

2) Lane-Independent Cost: The lane-independent output vector, is as follows [18]:

$$G = \begin{bmatrix} v - v_d, & \zeta - v_d, & 1 - \sum_{l=1}^{N_l} d_l^2 \end{bmatrix}^T, \quad (6)$$

where v_d is the desired velocity of the ego-vehicle and ζ is a slack variable to ensure a feasible and safe following distance during normal driving. The slack variable has the dynamics $\zeta_{k+1} = \zeta_k + u_\zeta \Delta t$, where u_ζ is its control variable. For a full description of the function of ζ, see [19]. The last element of G can be shown to have a minimum when a single lane decision variable is equal to 1 and all others are equal to 0, thereby penalizing tracking multiple lanes simultaneously.

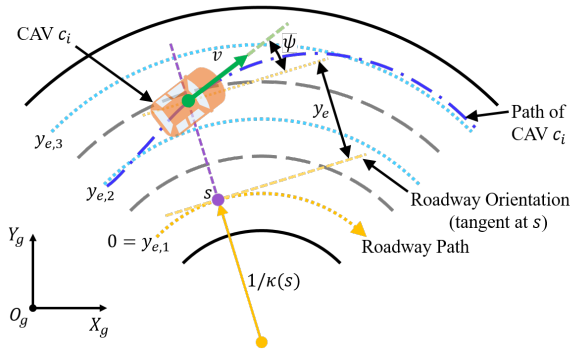

Fig. 3. Ego vehicle motion in the Frenet frame where s is the position along the path, $\kappa\left(s\right)$ is the road curvature as a function of s, ψ is the deviation angle from the heading direction, and O_g, X_g, and Y_g are the global origin, x-axis, and y-axis, respectively.

3) Predictability Cost: The predictability cost is utilized to ensure that CAV c_i does not deviate significantly from the prior plan shared with other CAVs c_p $(p \neq i)$ and its output vector is defined as [18]:

$$H = \begin{bmatrix} s - s^-, & y_e - y_e^- \end{bmatrix}^T, \quad (7)$$

where s^- and y_e^- are the synchronized position along the path and deviation from the lane centerline of the prior plan. The constant velocity synchronization method used is presented in [18].

4) Input Cost: The input cost penalizes the complete input vector $u = \begin{bmatrix} u_m, & u_\zeta, & u_1, & \cdots, & u_{N_l - 1} \end{bmatrix}^T$ in order to ensure that motions are smooth or comfortable, where u_m is the vector of inputs associated with the motion dynamics model.

B. Reference Speed Assignment

1) Rule-based Speed Assignment (RBSA): The RBSA seeks to assign the lane reference speed based on the immediate traffic surrounding CAV c_i; either reducing or increasing, respectively, the reference speed to that of a leading (ahead of and moving slower) or following (behind and moving faster) OV. The rules which govern the RBSA are presented in Algorithm 1 [18]. We omit the time index k to reduce clutter, however, it should be noted that Algorithm 1 is performed for each step of the horizon. First, for each lane l, the lane reference speed v_l is initialized at the unique base desired velocity v_{d_o} of CAV c_i. Then, for each ov_j in lane l, the RBSA identifies if ov_j is within a look-ahead distance Δs_{LA} of CAV c_i (Line 4), and if v_j, the velocity of ov_j, is lower than the current v_l or if v_l has not been modified from v_{d_o} (Line 5). If true, the RBSA checks if ov_j is leading, following, or alongside CAV c_i (Lines 6 and 7) and assigns v_l to be the minimum of v_j and the speed limit $\bar{v}$, accordingly.

Authorized licensed use limited to: CLEMSON UNIVERSITY. Downloaded on April 17,2022 at 23:29:03 UTC from IEEE Xplore. Restrictions apply.

Algorithm 1 Rule-based speed assigner

for each lane $l \in \mathcal{L}$ **do**
  $v_l = v_{d_o}$
  for each $ov_j \in \mathcal{E}$ on lane l **do**
    if $|s_i - s_j| < \Delta s_{LA}$ **and**
      $(v_j < v_l$ **or** $v_l = v_{d_o})$ **then**
        if $(s_i - s_j)\left(v_i - v_j\right) < 0$ **or**
          $|s_i - s_j| < \Delta s_{ij} + b\zeta$ **then**
            $v_l = \min\left(v_j, \quad \overline{v}\right)$
        end if
    end if
  end for
end for

2) Harmonization-based Speed Assignment (HSA): The lane reference speed is assigned in a distributed manner by estimating the average speed of traffic in each lane via on-board measurements and shared information. For each lane l, CAV c_i generates an estimate $\mu_{v,li} = \sum_{q=1}^{N_{v,li}} v_q / N_{v,li}$ of the average velocity of the $N_{v,li}$ vehicles in lane l within $\mathcal{F}_i$. Further, we assume the information matrix shared by each CAV c_p (using, for example, the collaborative perception schemes presented in [20]) will contain a limited amount of information about the traffic environment, i.e. $\mathbf{w}_p = \left\{w_p \quad \left\{\left[\mu_{v,lp} \quad \underline{r}_{lp} \quad \overline{r}_{lp} \quad N_{v,lp}\right]\right\}_{l\in\{1,\ldots,N_l\}}\right\}$. The sub-matrix w_p contains information used by the OVSP block (see Fig. 2). While the remaining elements $\underline{r}_{lp}$ and $\overline{r}_{lp}$ are the position of the forward and backward most OVs in $\mathcal{F}_p$ in each lane l, respectively, (see Fig. 1), and $N_{v,lp}$ is the number of vehicles on each lane l in $\mathcal{F}_p$. Using this information, we are able to obtain an improved estimate of the average velocity of traffic in a given lane via a weighted combination of $\mu_{v,li}$ and each shared estimate $\mu_{v,lp}$. It should be noted that the following calculations are made using data from the current time step.

To mitigate double counting vehicles, it is necessary to estimate the number of unique vehicles, $N_{u,lp}$, in $\mathcal{F}_p$. The following assumptions are necessary, in order to estimate $N_{u,lp}$ using only the shared information:

- the FOV in each lane l is a rectangle with width of lane l and with length bounded by $\underline{r}_{lp}$ and $\overline{r}_{lp}$,
- OVs are evenly distributed within the FOV in lane l.

It should be noted that more elaborate descriptions of the FOV are possible [21] at the cost of more complex computations. We then have:

$$N_{u,lp} = \frac{A_{u,lp}}{A_{lp}} N_{v,lp}, \tag{8}$$

where $A_{u,lp}$ is the unique FOV area of c_p in lane l, and A_{lp} is the total area of the FOV of c_p in lane l. The unique area $A_{u,lp}$ is calculated based on an ordered pairwise comparison of the bounds $\underline{r}_{li}$, $\overline{r}_{li}$, $\underline{r}_{lp}$, and $\overline{r}_{lp}$ for all CAVs $c_p \in \mathcal{C}_i$. The lane reference velocity v_l is then computed by CAV c_i as:

$$v_l = \frac{1}{N_{v,li} + \sum_{p=1}^{N_p} N_{u,lp}} \left[N_{v,li}\mu_{v,li} + \sum_{p=1}^{N_p} N_{u,lp}\mu_{v,lp} \right], \tag{9}$$

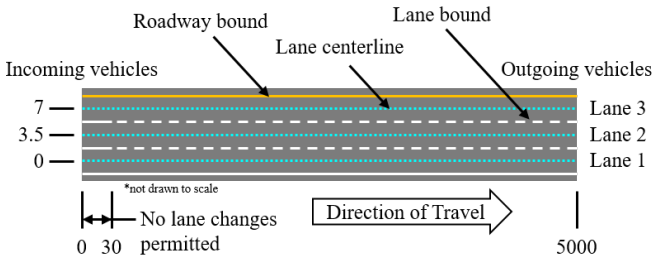

Fig. 4. Schematic of the freeway

where N_p is the number of CAVS communicating with c_i.

Each CAV then computes the desired velocity v_d, for both the RBSA and HSA schemes, based on the lane reference speed that is closest to v_{d_o}:

$$v_d = \arg\min_{v_l} |v_l - v_{d_o}|. \tag{10}$$

A simple search over the N_l lanes is used to solve (10). It should be noted that v_{d_o} is calculated by dividing CAV c_i's desired travel time on the link (designated by a higher level route planner) by the length of the link.

III. RESULTS AND DISCUSSIONS

In order to determine the effectiveness of the DMPC framework and the two variations of distributed speed assignment, the framework was implemented within the traffic microsimulation environment VISSIM [22]. The optimal control problem formulated above was solved using auto-generated code from the ACADO toolkit [23].

A. Simulation Setup

The analyzed freeway (or network), depicted in Fig. 4, consists of a 5km straight link with three 3.5m wide lanes and 0% road grade. Vehicles enter and exit the freeway at a single input and single output node located at the left- and right-most ends of the freeway, respectively. In order to minimize boundary effects on entrance, we restrict the vehicles from changing lanes for the first 30m of the freeway. The desired velocity of vehicles on the link is distributed about approximately 87km/hr utilizing the default VISSIM velocity distribution. Simulations begin with the freeway completely empty and last for 30 minutes of simulation time. To allow for the network to saturate, we omit the time from the start of the simulation scenario until the number of vehicles on the freeway reaches 90% of the maximum observed amount.

HDVs are assumed to follow the Wiedemann-99 (W-99) psycho-spacing car-following model [24]. The VISSIM default parameters were used, except for the standstill distance $CC0 = 3.04m$, and time headway $CC1 \sim \mathcal{N}(1.45, 0.1)$. For lane decisions, HDVs utilized VISSIM's default rule-based lane selection algorithm with default parameters [22].

We define CAV penetration rate (ρ) as the percentage of the traffic fleet that are CAVs. Additionally, we define traffic demand Q in vehicles per hour. In the following discussions, the subscripts v, d, and r pertain to the specific

Authorized licensed use limited to: CLEMSON UNIVERSITY. Downloaded on April 17,2022 at 23:29:03 UTC from IEEE Xplore. Restrictions apply.

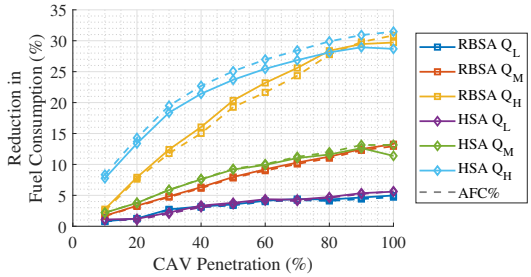

Fig. 5. Percent reduction in fuel consumption rate versus CAV penetration rate at traffic demands of $Q_L = 2000$, $Q_M = 4000$, and $Q_H = 6000$ veh/hr for both the RBSA and HSA cases.

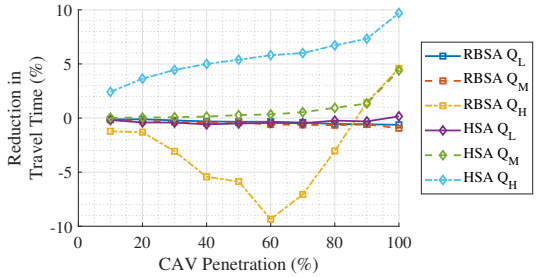

Fig. 6. Percent reduction in travel time versus CAV penetration rate at traffic demands of $Q_L = 2000$, $Q_M = 4000$, and $Q_H = 6000$ veh/hr for both the RBSA and HSA cases.

traffic demand Q_d, CAV penetration ρ_r, and reference speed assigner RSA_v, respectively. Specifically:

- $Q_d : d \in \{L, \quad M, \quad H\} \rightarrow \{2000, \quad 4000, \quad 6000\}$;
- $\rho_r : r \in \{1, \quad 2, \quad ..., \quad 10\} \rightarrow \{10, \quad 20, \quad ..., \quad 100\}$.
- $\text{RSA}_v : v \in \{R, \quad H\} \rightarrow \{\text{RBSA}, \quad \text{HSA}\}$;

Additional baseline simulations were completed with 0% CAV penetration and are designated with the subscript b along with the respective traffic demand subscript d.

B. Results

1) Fuel Consumption: CAVs offer a unique opportunity to reduce the consumption of fuel by mitigating unnecessary accelerations. To determine whether our proposed framework, with both RBSA and HSA, improves fuel economy, we analyze the average fuel consumption rate (L/100km) over each simulation run compared to the baseline. Fuel consumption is calculated using the methods and parameters presented in [25]. The observed percent reduction in average fuel consumption rate FC% is calculated as:

$$\text{FC\%}_{vdr} = 100\left(1 - \frac{\text{FC}_{vdr}}{\text{FC}_{bd}}\right), \tag{11}$$

where FC is the observed average fuel consumption rate of the entire fleet, CAVs and HDVs, for the given scenario.

In general, there is a trade-off between fuel consumption and travel time. In order to account for this, we introduce the required fuel consumption rate, RFC, or the fuel consumption rate required to maintain a constant velocity at the observed average velocity over an entire simulation. The time adjusted percent reduction in fuel consumption rate, AFC%, is then:

$$\text{AFC\%}_{vdr} = \text{FC\%}_{vdr} - 100\left(\frac{\text{RFC}_{vdr} - \text{RFC}_{bd}}{\text{FC}_{bd}}\right). \tag{12}$$

Based on this formulation, AFC% increases, compared to FC%, if travel time decreases concurrently and decreases if travel time increases.

Figure 5 shows $\text{FC\%}_{vd}$ (solid) and $\text{AFC\%}_{vd}$ (dashed) as a function of CAV penetration for both RSA methods. In general, there is a negligible difference between FC% and AFC% for low and medium traffic demands, Q_L and Q_M, respectively, with the exception of HSA at 100% CAVs and Q_M. There is also a negligible difference in performance between RBSA and HSA at Q_L and Q_M. At high traffic demand Q_H, however, the HSA consistently realizes an FC% and AFC% higher than RBSA at 40% CAVs and below. As CAV penetration increases over 40% CAVs, the fuel consumption benefits of HSA diminishes until at 100% CAVs, where HSA realizes only a marginal improvement over RBSA in AFC%. At high traffic demand, as CAV penetration increases, AFC% increases compared to FC% for HSA, whereas, RBSA does not follow this trend.

2) Travel Time: To see how AFC% correlates to travel times, we will define the percent reduction in travel time TT% in a similar manner to FC%:

$$\text{TT\%}_{vdr} = 100\left(1 - \frac{\text{TT}_{vdr}}{\text{TT}_{bd}}\right), \tag{13}$$

where TT is the average travel time observed over the simulation scenario. Figure 6 presents $\text{TT\%}_{vd}$ as a function of CAV penetration. For both RSA methods at Q_L and for RBSA at Q_M, there is a negligible change in travel time with respect to the baseline scenario. However, HSA at Q_M realizes marginal improvements from 50% to 90% CAVs, and significant improvements at 100% CAVs. The performance gap between RBSA and HSA is even larger at high traffic demand Q_H. HSA realizes improvements at all levels of CAV penetration, ranging from 2% to 10%. RBSA at high traffic demand, however, results in a significant increase in travel time at CAV penetrations below 90%, with TT% ranging from -1% to -10%. When CAV penetration reaches $\geq 90\%$, RBSA starts to see an improvement in travel time equivalent to the level of HSA at low CAV penetrations.

The difference in travel time between the RBSA and HSA approaches may be attributed to the inherent differences in the reference speed assigners; the rules within the RBSA are designed so that in dense traffic the lowest observed velocity of vehicles leading or following CAV c_i is assigned as v_l for a given lane l, whereas the HSA assigns v_l to be the estimated average speed in the lane. It is important to note that in order to avoid the DMPC planner choosing multiple lanes simultaneously, lane reference speed tracking is weighted higher than desired velocity tracking, therefore lane reference speed tracking dominates. We will also note, that as the length of the network is fixed, and there is only one route through the network, discussing average observed velocity over the length of the simulation is equivalent to discussing average travel time. To better understand the difference in RSA methods, we examine the spatial speed

Authorized licensed use limited to: CLEMSON UNIVERSITY. Downloaded on April 17,2022 at 23:29:03 UTC from IEEE Xplore. Restrictions apply.

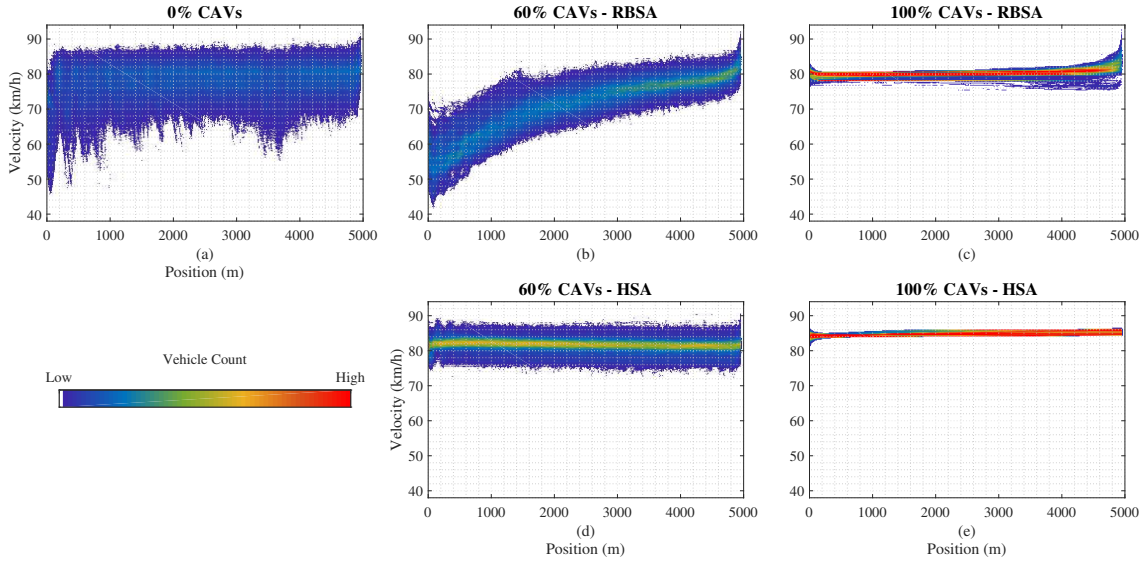

Fig. 7. Position-velocity state measurement pair density plot with a traffic demand of 6000 veh/hr for select CAV penetrations and RSA types; (a) baseline scenario, (b) RBSA at $\rho_6 = 60\%$ CAVs, (c) RBSA at $\rho_{10} = 100\%$ CAVs, (d) HSA at $\rho_6 = 60\%$ CAVs, (e) HSA at $\rho_{10} = 100\%$ CAVs.

harmonization. Figure 7 presents vehicle counts at position-velocity pairs for the case of high traffic demand Q_H. In dense traffic, as a downstream vehicle brakes, the disturbance can move upstream and sometimes magnify. Although RBSA CAVs have a smoothing effect on the traffic, the population of CAVs tend to slow more than an equivalent population of HDVs, as v_l is assigned to be the lowest observed downstream velocity. This effect is most prominent at 60% CAVs when there is still a significant number of HDVs causing braking disturbances and an insufficient number of CAVs to smooth the disturbances, as seen by comparing Fig. 7(a) and (b). At lower penetrations, the traffic is governed more by HDVs so TT% increases. Similarly, as more CAVs are introduced at higher penetrations, the disturbances from fewer HDVs in traffic are smoothed, until at 100% CAVs the disturbances from HDVs are removed and the smoothing effect results in an improved TT over the baseline. The HSA approach smooths traffic more efficiently than the RBSA approach, as it assigns the estimated average velocity, instead of the lower extreme, as seen when comparing Fig. 7(d) to (b). Finally, from Figs. 7(c) and (e), at 100% CAVs penetration, we observe that the HSA CAVs settle to a velocity closer to the mean of the desired velocity distribution (87km/hr), than the RBSA CAVs, which track a lower end of the desired velocity distribution (80km/hr).

3) Lane Changes: To analyze the impact the two RSA methods have on lane decisions, we plot the average number of lane changes per vehicle ($\mathrm{N_{LC}}$/veh) in Fig. 8. The maximum $\mathrm{N_{LC}}$/veh is observed at Q_M, as can be seen by comparing the baselines in Figs. 8(a), (b), and (c). At low demands, lane changes are infrequent as there are not many vehicles to impede motion and make lane changes beneficial. Conversely, at high demand the traffic is too dense, therefore, a safe lane change is not possible. For both RBSA and HSA at all traffic demands, as CAV penetration increases the number of lane changes per vehicle for the fleet decreases until it approaches or reaches 0 at 100% CAVs.

Now we will focus on how the distributed CAVs impact the lane decisions of HDVs within the traffic. In Fig. 8(a), for both RSA approaches, the lane changes per HDV decreases at similar rates as CAV penetration increases. Then, as CAV penetration increases in Fig. 8(b), the number of lane changes per HDV for both RSA methods reduces at approximately the same rate, however, the HDVs in the HSA case change lanes on average roughly 0.2 fewer times. The difference is greater at Q_H (Fig. 8(c)), as the HDVs in the HSA case change lanes on average 0.3 fewer times. A noteworthy observation in Fig. 8(c) is that, with RBSA CAVs, the HDVs change lanes more frequently than the baseline at CAV penetrations $\leq 60\%$. RBSA CAVs maintain larger following distances and are traveling on average slower than a population of HDVs, therefore incentivizing lane changes and leading to an increase in lane changes per vehicle.

Lastly, we will analyze how the CAVs themselves change lanes. Across all traffic demand levels CAVs utilizing the RBSA change lanes more frequently than CAVs using the HSA. The average speed in a given lane is subject to the distribution of the desired velocity of vehicles in that lane. Since there is no difference in the distribution of desired velocities for vehicles populated in each lane, the average speed will trend towards the same mean. As a result, there is little incentive to change lanes for HSA CAVs, as noted by the fact that the $\mathrm{N_{LC}}$/veh is less than $0.2\mathrm{N_{LC}}$/veh for all scenarios. Conversely, as the RBSA assigns the extremes of the observed velocity, it is more likely that the DMPC will decide that a lane change is cost effective. Therefore, at lower penetrations, particularly at higher demands, significantly more lane changes are observed. Still, as CAV penetration increases the incentive to change lanes reduces, as all RBSA CAVs are governed by the same control framework with each

Authorized licensed use limited to: CLEMSON UNIVERSITY. Downloaded on April 17,2022 at 23:29:03 UTC from IEEE Xplore. Restrictions apply.

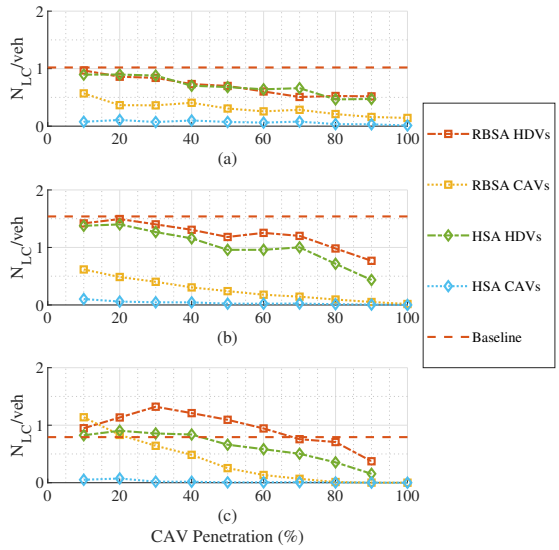

Fig. 8. Number of lane changes per vehicle versus % CAV penetration at traffic demands (a) $Q_L = 2000$, (b) $Q_M = 4000$, and (c) $Q_H = 6000$ veh/hr.

CAV only having a unique v_{d_o}.

IV. CONCLUSIONS

In this paper, we have proposed a distributed approach for harmonizing speed with a two-dimensional distributed motion planner for CAVs. By implementing the approach in large scale microscopic traffic simulations we have shown how an appropriately designed distributed control framework for CAVs can improve fuel consumption and traffic flow. We capped off the discussion with an investigation into how reference speed assignment impacts the incentives to change lanes.

On-going investigations are looking at how the distributed control framework with both the RBSA and HSA perform when a bottleneck is introduced in the network, in particular, a speed reduction zone. A shortcoming of the HSA is that it only estimates the instantaneous average velocity on a given lane. Future work will investigate a more complete traffic state estimation that will account for predicted lane choices of the ego-vehicle and object vehicles, as well as, the uncertainties in shared state estimates.

REFERENCES

[1] D. Schrank, B. Eisele, and T. Lomax, "2019 Urban Mobility Report," Texas A&M Transportation Institute, Tech. Rep., 2019. [Online]. Available: https://static.tti.tamu.edu/tti.tamu.edu/documents/mobility-report-2019.pdf

[2] D. Dolgov, S. Thrun, M. Montemerlo, and J. Diebel, "Practical search techniques in path planning for autonomous driving," *International Symposium on Combinatorial Search, SoCS 2008*, pp. 32–37, 2008.

[3] R. Schubert, U. Scheunert, and G. Wanielik, "Planning feasible vehicle manoeuvres on highways," *IET Intelligent Transport Systems*, vol. 2, no. 3, p. 211, 2008.

[4] K. Berntorp and S. Di Cairano, "Joint Decision Making and Motion Planning for Road Vehicles Using Particle Filtering," *IFAC-PapersOnLine*, vol. 49, no. 11, pp. 175–181, 2016.

[5] K. Berntorp, P. Inani, R. Quirynen, and S. Di Cairano, "Motion planning of autonomous road vehicles by particle filtering: Implementation and validation," in *2019 American Control Conference (ACC)*. IEEE, 2019, pp. 1382–1387.

[6] Q. Wang, B. Ayalew, and T. Weiskircher, "Optimal assigner decisions in a hybrid predictive control of an autonomous vehicle in public traffic," in *2016 ACC*, vol. 2016-July. IEEE, jul 2016, pp. 3468–3473. [Online]. Available: https://doi.org/10.1109/ACC.2016.7525450

[7] M. A. S. Kamal, S. Taguchi, and T. Yoshimura, "Efficient driving on multilane roads under a connected vehicle environment," *IEEE Transactions on Intelligent Transportation Systems*, vol. 17, no. 9, pp. 2541–2551, 2016.

[8] R. A. Dollar and A. Vahidi, "Predictively Coordinated Vehicle Acceleration and Lane Selection Using Mixed Integer Programming," in *Proceedings of the ASME 2018 DSC Conference. Volume 1*. Atlanta, Georgia, USA: ASME, sep 2018.

[9] D. D. Yoon and B. Ayalew, "Social Force Control for Human-Like Autonomous Driving," in *Proceedings of the ASME 2018 IDETC & CIE Conference*. ASME, aug 2018.

[10] Q. Wang, T. Weiskircher, and B. Ayalew, "Hierarchical Hybrid Predictive Control of an Autonomous Road Vehicle," in *Proceedings of the ASME 2015 DSC Conference. Volume 3*. ASME, Oct 2015. [Online]. Available: https://doi.org/10.1115/DSCC2015-9773

[11] Q. Wang, B. Ayalew, and T. Weiskircher, "Predictive Maneuver Planning for an Autonomous Vehicle in Public Highway Traffic," *IEEE Transactions on Intelligent Transportation Systems*, vol. 20, no. 4, pp. 1303–1315, apr 2019. [Online]. Available: https://doi.org/10.1109/TITS.2018.2848472

[12] C. Fuhs and P. Brinckerhoff, "Synthesis of active traffic management experiences in europe and the united states," United States. Federal Highway Administration, Tech. Rep., 2010.

[13] G.-L. Chang, S. Y. Park, and J. Paracha, "Intelligent transportation system field demonstration: integration of variable speed limit control and travel time estimation for a recurrently congested highway," *Transportation Research Record*, vol. 2243, no. 1, pp. 55–66, 2011.

[14] G. H. Bham, S. Long, H. Baik, T. Ryan, and L. Gentry, "Evaluation of Variable Speed Limits on I-270 / I-255 in St . Louis," Missouri Department of Transportation, Jefferson City, MO, Tech. Rep., 2010.

[15] A. Talebpour, H. S. Mahmassani, and S. H. Hamdar, "Speed Harmonization: Evaluation of Effectiveness Under Congested Conditions," *Transportation Research Record*, vol. 2391, no. 1, pp. 69–79, jan 2013.

[16] J. Ma, X. Li, S. Shladover, H. A. Rakha, X.-Y. Lu, R. Jagannathan, and D. J. Dailey, "Freeway Speed Harmonization," *IEEE Transactions on Intelligent Vehicles*, vol. 1, no. 1, pp. 78–89, mar 2016.

[17] A. A. Malikopoulos, S. Hong, B. B. Park, J. Lee, and S. Ryu, "Optimal Control for Speed Harmonization of Automated Vehicles," *IEEE Transactions on Intelligent Transportation Systems*, vol. 20, no. 7, pp. 2405–2417, jul 2019.

[18] N. Goulet and B. Ayalew, "Coordinated Model Predictive Control on Multi-Lane Roads," in *Proceedings of the ASME 2019 IDETC & CIE Conference*. Anaheim, CA, USA: ASME, aug 2019, pp. 1–8. [Online]. Available: https://doi.org/10.1115/DETC2019-98117

[19] T. Weiskircher, Q. Wang, and B. Ayalew, "Predictive Guidance and Control Framework for (Semi-)Autonomous Vehicles in Public Traffic," *IEEE Transactions on Control Systems Technology*, vol. 25, no. 6, pp. 2034–2046, nov 2017. [Online]. Available: https://doi.org/10.1109/TCST.2016.2642164

[20] D. D. Yoon, G. G. M. N. Ali, and B. Ayalew, "Data Association and Fusion Framework for Decentralized Multi-Vehicle Cooperative Perception," in *Proceedings of the ASME 2019 IDETC & CIE Conference*. Anaheim, CA, USA: ASME, aug 2019.

[21] J. Liu, P. Jayakumar, J. L. Stein, and T. Ersal, "A nonlinear model predictive control formulation for obstacle avoidance in high-speed autonomous ground vehicles in unstructured environments," *Vehicle System Dynamics*, vol. 56, no. 6, pp. 853–882, 2018.

[22] PTV Group, "PTV Vissim 10 User Manual," 2018.

[23] B. Houska, H. J. Ferreau, and M. Diehl, "An auto-generated real-time iteration algorithm for nonlinear MPC in the microsecond range," *Automatica*, vol. 47, no. 10, pp. 2279–2285, oct 2011.

[24] G. Liu, "W99 Car Following Model; How It Works," 2016. [Online]. Available: http://w99demo.com/w99demo_ptv_ugm.pdf

[25] R. A. Dollar and A. Vahidi, "Quantifying the impact of limited information and control robustness on connected automated platoons," in *2017 IEEE 20th International Conference on Intelligent Transportation Systems (ITSC)*. IEEE, 2017, pp. 1–7.

Authorized licensed use limited to: CLEMSON UNIVERSITY. Downloaded on April 17,2022 at 23:29:03 UTC from IEEE Xplore. Restrictions apply.